



Magnetically enhanced electrochemical conversion of CO₂ to formate: Experimental studies

Jose Antonio Abarca^{a,*}, Xian Wu^b, Cristina González-Fernández^a, Ioannis H. Karampelas^c, Alejandro Gutierrez-Carballo^d, Joseph A. Gauthier^d, Gerardine G. Botte^d, Jose Solla-Gullon^e, Angel Irabien^a, Guillermo Díaz-Sainz^{a,*}, Jenifer Gomez-Pastora^{d,*}

^a Departamento de Ingenierías Química y Biomolecular, Universidad de Cantabria, Avenida de los Castros s/n, 39005 Santander, Spain

^b Boston Institute of Biotechnology, Southborough, MA 01772, United States

^c Nematik USA, Inc., Sheboygan, WI 53081, United States

^d Department of Chemical Engineering, Texas Tech University, Lubbock, TX 79409, United States

^e Instituto de Electroquímica, Universidad de Alicante, Apdo. 99, Alicante E-03080, Spain

ARTICLE INFO

Keywords:

CO₂ electroreduction
Magnetic field
Formate
Gas diffusion electrode

ABSTRACT

The application of external magnetic fields in electrochemical processes has emerged as a promising strategy to enhance efficiency. Nevertheless, the use of magnetic fields in electrochemical CO₂ reduction (ERCO₂) has been scarcely explored. This study evaluates the impact of magnetic fields on ERCO₂ to formate in a filter-press reactor, combining experimental analysis with magnetic field modeling to understand the performance enhancements achieved by placing magnets outside the electrochemical cell. Magnetic field modeling reveals that the positioning of magnets relative to the cathode surface significantly affects the field strength. For instance, placing a magnet near the anode generates a field strength of 20 mT on the GDE, while positioning two magnets at opposite ends of the cell increases the field to 400 mT. Experimentally, placing magnets near the cathode or at both ends of the cell boosts formate concentration by more than 20 %, achieving values of 4.4 g L⁻¹ and 4.95 g L⁻¹, respectively, with FEs approaching 100 %. These improvements are attributed to the magnetohydrodynamic (MHD) effect, which enhances mass transfer by inducing turbulence in the cathodic electrolyte. This effect is particularly important at low catholyte flow rates, leading to a more than 50 % increase in formate concentration, reaching up to 27.25 g L⁻¹ at a flow rate of 0.07 mL min⁻¹ cm⁻². However, the application of magnetic fields also increases energy consumption due to the higher cell voltage requirements, as indicated by Tafel analysis. Despite this limitation, this study demonstrates the potential application of magnetic fields to enhance ERCO₂ processes, paving the way for future research to further explore and optimize this promising strategy.

1. Introduction

Electrocatalytic reduction of carbon dioxide (ERCO₂) holds great promise as a technology for converting CO₂ into value-added chemicals, offering a potential strategy to mitigate climate change [1–4]. ERCO₂ can yield several products, including methanol, carbon monoxide, formic acid or multicarbon (C₂₊) products [5–7]. Formic acid or formate (depending on pH) are particularly attractive carbon-based products. They are excellent fuels for direct formic acid or formate fuel cells, serve as efficient hydrogen storage media, and have broad industrial applications [2,8–10]. Consequently, ERCO₂ to formic acid/formate has emerged as an exciting area of research, with significant advancements

in catalysts, electrodes, reactor configurations and operational conditions over recent decades. These developments have enabled formate concentrations exceeding 35 %wt, high Faradaic efficiencies toward this product (80–90 %), and energy consumptions below 200 kWh·kmol⁻¹ [5,11–15].

However, ERCO₂ faces critical challenges that remain unsolved and that considerably compromise its performance [16]. These include the limitation in reaction rates due to CO₂ mass transfer and difficulties in maintaining high current densities (> 200 mA·cm⁻²), which are essential for industrial relevance [4,16–18].

Coupling magnetic fields with electrochemistry represents a promising approach for boosting electrochemical reactions [19–21]. In this

* Corresponding authors.

E-mail addresses: joseantonio.abarca@unican.es (J.A. Abarca), guillermo.diazsainz@unican.es (G. Díaz-Sainz), Jenifer.Gomez@ttu.edu (J. Gomez-Pastora).

<https://doi.org/10.1016/j.cej.2025.163614>

Received 8 January 2025; Received in revised form 27 April 2025; Accepted 9 May 2025

Available online 10 May 2025

1385-8947/© 2025 The Author(s). Published by Elsevier B.V. This is an open access article under the CC BY-NC license (<http://creativecommons.org/licenses/by-nc/4.0/>).

regard, magnetic fields can alleviate mass transfer limitations in ER_{CO}₂ through the magnetohydrodynamic (MHD) effect [16]. This effect involves the generation of macroscopic and microscopic convection in the electrolyte due to the interaction of the magnetic field with current density, driven by the Lorentz force [16,19,20,22,23]. The induced convection enhances mass transport, promoting a continuous supply of electroactive species to the electrode surface, thereby boosting ER_{CO}₂ performance [16,24,25]. A comprehensive explanation of the MHD effect is provided in these excellent works [19,20,26].

Despite the outstanding potential of the MHD effect in electrochemical processes, few studies have exploited its application for CO₂ conversion, primarily focusing on enhancing ER_{CO}₂ to carbon monoxide [27–29]. These studies investigated changes in current density and potential when magnets were positioned outside the cell (H-type, single compartment) near the anode or cathode. For instance, Karki et al. [29] and Kodaimati et al. [28] observed variations in velocity vectors and pH around the working electrode (Cu and Ag) in H-type cells under magnetic fields (0.2–0.3 T). These studies demonstrate that magnetic fields can influence CO₂ conversion.

Expanding the application of the MHD effect to produce other valuable products like formic acid/formate is worthwhile given their industrial importance. Additionally, the limited number of studies on magnetically enhanced ER_{CO}₂ highlights the need for deeper understanding of how magnetic fields impact CO₂ conversion, particularly in electrolyzers with different cathode configurations. Among these, gas diffusion electrodes (GDEs) are especially promising. GDEs improve contact between the gas, catalyst, and electrolyte, significantly enhancing ER_{CO}₂, as shown in our previous studies [11,30]. However, to the best of our knowledge, no studies have reported the influence of magnetic fields on CO₂ conversion to formate using GDE as the cathode in a continuous mode. Since GDEs enable operation at industrially relevant current densities (200 mA·cm⁻²), exploring the effect of magnetic fields on ER_{CO}₂ using this cathode configuration represents a compelling area of study.

In this context, the present work aims to investigate the effect of magnetic fields on ER_{CO}₂ to formate in continuous mode using GDE as cathode in a flow-cell electrolyzers. An electrochemical flow reactor containing bismuth/carbon-based GDEs was employed, as bismuth catalysts exhibit high selectivity towards formate [11,30]. The study evaluates how magnet placement (anode, cathode, or both ends) and catholyte flow rates influence magnetically coupled CO₂ conversion to formate. Several figures of merit including formate concentration and rate, Faradaic efficiency (FE), and energy consumption were analyzed to address this investigation. Collectively, the insights gained from this work evidenced the potential of magnetic fields for boosting ER_{CO}₂ to formate, paving the way for the design of optimized electrolyzers that exploit the MHD effect for CO₂ conversion.

2. Methodology

2.1. Electrode fabrication

For the cathode, a Bi-Gas Diffusion Electrode (GDE) is used as the working electrode to carry out the CO₂ electrochemical reduction to formate. These electrodes, with a geometric surface area of 10 cm², are composed of a Gas Diffusion Layer (GDL), specifically Sigracet 39 BB (Fuel Cell Store), coated with a bismuth-based catalyst (Bi/C) on the substrate. Bismuth is selected due to its proven efficacy in converting CO₂ to formate in previous studies [10,30,31].

The GDEs are fabricated using an automatic spray pyrolysis technique (ND-DP Mini Ultrasonic Spray Coater, Nadetech Innovations), optimized to ensure high reproducibility and performance [32]. During the fabrication process, catalytic ink is deposited onto the carbonaceous support to reach a catalyst loading of 0.75 mg cm⁻². The catalytic ink is composed of Bi/C nanoparticles suspended in isopropanol (laboratory reagent grade, ≥99.5 %, Fischer Chemicals) as a solvent (97 % wt.) with

Nafion ionomer (D521, 5 % wt. dispersion, Ion Power) as a binder, maintaining a catalyst/ionomer ratio of 70/30. Both catalyst and fabricated GDEs have been previously characterized [10].

2.2. Magnetic field sources and magnetic field and MHD simulations

For experimental tests, different magnet configurations are employed. On the cathode side, a magnet array consisting of five identical magnets with dimensions of 30x10x4 mm³ is arranged, covering a total volume of 50x30x4 mm³ (length, width, depth). This magnet assembly is used to be able to cover all the GDE external area so that the magnetic field can affect a bigger volume in the cathodic compartment in comparison to a single magnet of the same dimensions. On the anode, a single magnetic block with dimensions of 40x18x5 mm³ is used. Fig. 1 a) presents the experimental setup, showing the placement of magnets on both electrodes. All magnets were commercially sourced at the highest available grades (N52, N35) and manufactured from rare earth metal alloys (NdFeB).

The magnetic fields generated around the electrodes for various magnet configurations are simulated using the finite-element method (FEM) in COMSOL Multiphysics 6.2 software, as described in our previous studies [33,34]. Three scenarios are modeled: (i) a magnetic assembly located on the cathode side only, (ii) a magnetic assembly located on the anode side only, and (iii) magnet assemblies positioned on both electrodes. Fig. 1 b) presents the simulated geometry for the third scenario, with magnets placed adjacent to both electrodes, including their dimensions and polarities (north and south poles indicated by letters N and S, respectively).

Once the geometry is established, magnetic material properties are assigned, and magnetic flux conditions are configured. To account for the entire electrolyzer system, an additional surrounding domain is introduced, modeled as air. A finer mesh is applied through the system to improve accuracy. To characterize the magnetic field, the “magnetic fields, no currents (mfnc)” physics interface within the AC/DC module is used across all domains. Briefly, the simulations are based on Maxwell’s equations under the magnetostatic approximation, assuming no time-varying electric fields and no currents. The governing equations in the “magnetic fields, no currents” (mnfc) interface are:

$$\nabla \cdot \mathbf{B} = 0 \quad (1)$$

$$\nabla \times \mathbf{H} = 0 \quad (2)$$

where $\mathbf{B} = \mu_0(\mathbf{H} + \mathbf{M})$, and \mathbf{M} is the magnetization of the NdFeB permanent magnets. We model the magnetization as a uniform vector field within the magnets, based on manufacturer-supplied remanent magnetization values. The magnetic insulation ($\mathbf{n} \cdot \mathbf{B} = 0$) on the external boundaries of the air domain is chosen to simulate an open magnetic field. Continuity of the magnetic vector potential is enforced at all material interfaces. The simulations assume negligible eddy currents and displacement currents due to the static nature of the magnetic field and the non-conductive surrounding medium (air). As such, the time-varying and conductive effects are omitted, justifying the use of the mfnc module. We have validated this model in our previous publications using experimental data [34]. This simulation provided the magnetic flux density (\mathbf{B}) within the system.

Additionally, the electrolyte in the cell will experience a volume force (Lorentz force) as a consequence of the interaction between the ionic current and the magnetic field. We have included the effects of these forces in the fluid flow behavior in the catholyte compartment (that was modeled using a laminar flow approach), to predict the effect of the field in the generation of the MHD effect. Briefly, the magnets set up a static magnetic field \mathbf{B} , that induce currents \mathbf{J} in the fluid following the equation:

$$\mathbf{J} = \sigma (\mathbf{v} \times \mathbf{B}) \quad (3)$$

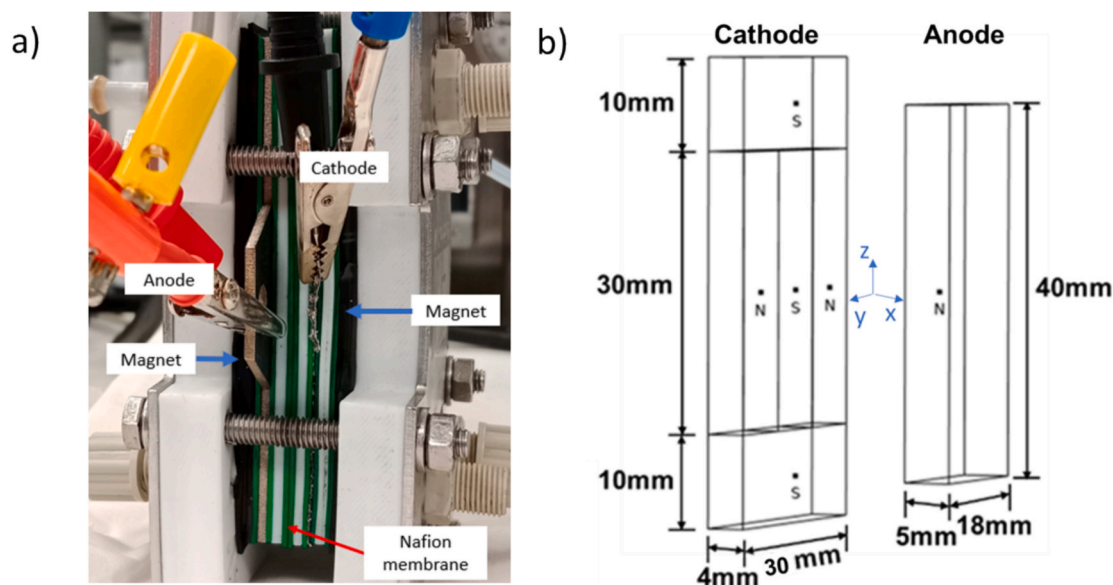


Fig. 1. a) Experimental setup showing the magnet positions at the cathode and anode sides. b) simulated geometry for calculating the magnetic fields inside the electrolyzer, depicting magnet dimensions and origin of coordinate system.

where σ is the conductivity of the fluid, and \mathbf{v} the velocity. This current \mathbf{J} , flowing through the magnetic field, leads to a volume force on the fluid equal to:

$$\mathbf{F} = \mathbf{J} \times \mathbf{B} \quad (4)$$

These equations were solved using the “magnetic and electric fields” and “laminar flow” modules of COMSOL Multiphysics.

2.3. Filter press tests experiments

The prepared Bi-GDEs serve as working electrodes in a continuous system within a filter press electrochemical cell, operating in single-pass mode for reactant flow. The experimental setup includes the filter press cell (Micro Flow Cell, ElectroCell A/s), peristaltic pumps (HF-LabN3-III, HygiaFlex), tanks, and a potentiostat-galvanostat (Arbin Instruments, MSTAT4), as shown in Fig. 2.

Fig. 1.a and 3 represent a scheme of the cell. Two internal configurations were tested. The first is a liquid-liquid configuration, where both the cathode and anode compartments contain liquid electrolytes, separated by a cation exchange membrane, Nafion 117. This membrane allows cations to transfer from the anode to the cathode compartment. In

this setup CO_2 reduction occurs at the cathode, where pure CO_2 is supplied in the gas phase at a flow rate of 200 mL min^{-1} , allowing it to pass through the GDE to reach the catalyst surface and the liquid electrolyte. The catholyte is a $0.5 \text{ M KCl} + 0.45 \text{ M KHCO}_3$ solution, with different catholyte flow rates per geometric surface area ($0.07, 0.15, \text{ and } 0.57 \text{ mL min}^{-1} \text{ cm}^{-2}$).

The anolyte in the anodic compartment is a 1 M KOH solution with a flow rate per geometric surface area of $0.57 \text{ mL min}^{-1} \text{ cm}^{-2}$. A dimensionally stable anode, [DSA/ O_2 (Ir- MMO (mixed metal oxide) on platinum)] is used as the counter electrode, while a leak-free Ag/AgCl 3.4 M KCl reference electrode is positioned near the working electrode in the cathode compartment.

Experiments are performed with magnets positioned in various configurations. In single-magnet setups, one magnet is placed near either the cathode or the anode. In double-magnet setups, magnets are placed on both anode and cathode sides, covering the reactor’s active area.

In the gas-liquid configuration, the liquid catholyte is omitted by placing the GDE in direct contact with the ion exchange membrane, and a humidified CO_2 stream of 200 mL min^{-1} is supplied to the compartment.

All experiments are conducted for 3600 s experiments at ambient

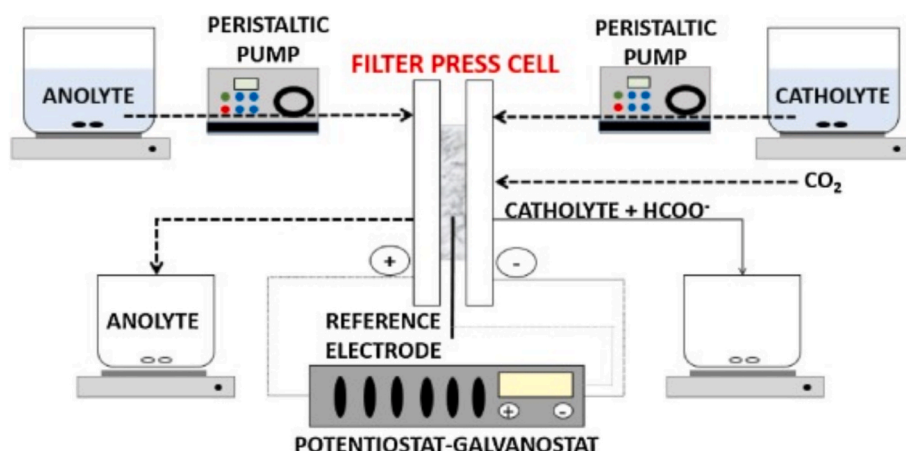


Fig. 2. Experimental setup for Bi-GDE tests in continuous CO_2 electrocatalytic reduction to formate. Adapted with permission from [10].

pressure (101,325 Pa) and room temperature (20 °C). The key variables examined are the catholyte flowrate (Q/A), and the current density (j), supplied by the potentiostat–galvanostat. Samples are taken every 30 min in duplicate for analysis. Formate concentration is measured using an ion chromatograph (Dionex ICS 1100 equipped with an AS9 – HC column, using Na_2CO_3 as the eluent).

The performance of CO_2 electroreduction to formate is evaluated using the following figures of merit (Eqs. (1)–(3)) [5,35]:

- Faradaic Efficiency (FE) quantifies the portion of current utilized to produce formate:

$$FE(\%) = \frac{z \cdot M \cdot F}{j \cdot A \cdot t} \times 100 \quad (5)$$

where z is the number of electrons exchanged in the reduction reaction (2 for formate), M is the moles of formate produced, F is the Faraday constant (96485 C mol^{-1}), j is the applied current density, t refers to the experimental time, and A is the geometric active area.

- Formate Rate (r) measures formate formation per time and area:

$$r \left(\frac{\text{mmol}}{\text{m}^2 \text{s}} \right) = \frac{M}{t \cdot A} \quad (6)$$

where M and A are as defined above, and t is the experiment duration.

- Energy Consumption (EC) indicates the total energy required to produce one kilomole of formate:

$$EC \left(\frac{\text{kWh}}{\text{kmol}} \right) = \frac{j \cdot A \cdot V \cdot t}{M} \quad (7)$$

where j , A , t , and M are as in Eqs. (1) and (2), and V is the applied potential.

The electrochemical performance of the system under a magnetic field is evaluated using Tafel analysis, varying the applied current density from 25 to 200 mA cm^{-2} , with and without the presence of magnets. During this process, both cathode and cell potential are recorded to generate Tafel plots. The cathode potential is measured with the potentiostat, as the three-electrode set up allows the continuous data recording, while the cell potential is determined by using a multimeter.

3. Results

3.1. Evaluation of the different magnet positions

3.1.1. Field simulations

Fig. 4.a presents the magnetic field distribution (b field vectors) inside the electrolyzer for the three magnetic field configurations tested in this study. Additionally, in Fig. 4.b we present 2D maps (x-z) of the magnetic field (B magnitude, in Tesla) inside the electrolyzer, while Fig. 4.c depicts the magnetic field distribution at the cathode (on the GDE surface) for three scenarios: magnet on both electrodes (left), magnet only on the cathode (center) and magnet only on the anode side (right).

On the one hand, minimal variations in the magnitude of the magnetic field across the cathodic compartment or on the cathode itself are observed when the magnet is placed either on both electrodes or only at the cathode side. We have calculated the B field as a function of z in that particular plane (Fig. S.1), and the average field for these two scenarios is very similar, with values around 200 mT. The main difference between the two cases is the smoother B field for the scenario where the magnet is only at the cathode (low and high values of 150 and 300 mT, respectively), in comparison to the lower/higher values achieved for the condition where magnets are on both ends (100 mT and 350 mT, respectively). The different field conditions also cause a slightly varying

distribution of the B field vectors (presented in Fig. 4.a), which affects mass transfer dynamics in the electrolyzer. Indeed, as it can be noticed from Fig. 4.a, the direction of the vectors within the cathodic compartment is slightly different between both scenarios, with vectors mainly pointing toward the GDE surface for the case where magnet is only placed on the cathode, and with vectors pointing in a variety of directions in the electrolyzer volume for the scenario where magnets are placed on both ends. Nevertheless, when the magnet is only located on the anode, negligible magnetic field values are achieved (20 mT) within the cathodic volume. Fig. 4.b also presents the variation of the magnetic field across the width of the electrolyzer, showing how the magnetic field diminishes drastically with increasing distance from the magnet poles, as expected. Overall, these results suggest that the process can be enhanced by placing magnets either only on the cathode or on both electrodes, due to the favorable magnetic field configurations achieved for these scenarios, with slightly different values and B field vectors achieved for these two conditions.

3.1.2. Effect of the magnet position in ERCO_2 to formate

Different experiments are performed to evaluate the impact of the magnetic field created by the magnets on the electrochemical CO_2 reduction to formate behavior. Initially, the effect of the magnet is assessed by performing continuous CO_2 conversion at 200 mA cm^{-2} with the magnets positioned near the cathode, the anode, or at both ends of the electrochemical cell (Fig. 3). Results from the CO_2 to formate conversion performance are shown in Fig. 5.

As observed in Fig. 5, the positioning of the magnet in the electrochemical cell influences CO_2 conversion to formate in various ways. For instance, placing the magnet next to the anode yields results similar to those obtained without magnets, with a formate concentration of 3.85 g L^{-1} and FE of 78.4 %, compared to 3.95 g L^{-1} and 80.4 % without magnets. In this configuration, the greater distance from the cathode surface, where CO_2 reduction reaction takes place, minimizes magnetic field's influence. However, when the magnet is positioned next the working electrode, a significant improvement in formate production is observed, reaching 4.4 g L^{-1} with an FE of 89.6 %, indicating that the magnetic field is directly enhances the CO_2 reduction reaction at the cathode surface. Additionally, placing magnets at both ends of the reactor creates a combined magnetic field effect, which further intensifies the reaction at the cathode surface. This configuration yields a formate concentration of 4.95 g L^{-1} , improving conversion performance by 20 % over the system without magnets. The selectivity towards formate is also enhanced, achieving a FE of nearly 100 % (99.6 %). This enhancement can be attributed to the MHD effect [36], where the magnetic field induces mixing in the electrolyte compartment, reducing the mass transfer resistance of charge species toward the electrode surface and accelerating reaction kinetics [16].

Additionally, we have calculated the velocity values of the electrolyte in the cathodic compartment for all the magnet configurations tested, as well as for the case when there is not a magnetic field applied. Fig. 6.a presents the electrolyte velocity values on the GDE surface, as well as 1 mm away from the cathode (Fig. 6.b) for a representative flow rate value. It can be seen that the presence of the magnetic field enhances mass transport via MHD effects, as the velocity on the cathode surface is particularly increased when there is a magnetic field applied in the electrolyzer, in comparison to the case where no magnetic field is generated (Fig. 6.a). This is particularly significant for the cases where the magnet is located on the cathode (either alone, or at both ends), especially for high z values on the GDE surface. The higher velocity values on the GDE surface are directly correlated to a higher conversion of CO_2 to formate.

Fig. 7 presents performance results in terms of formate production rate and energy consumption. The formate production rate trends similarly to formate concentration, with magnets in the electrochemical cell enhancing reaction kinetics. A production rate of 10.4 $\text{mmol m}^{-2} \text{s}^{-1}$ is achieved with magnets are placed at both ends of the cell. However,

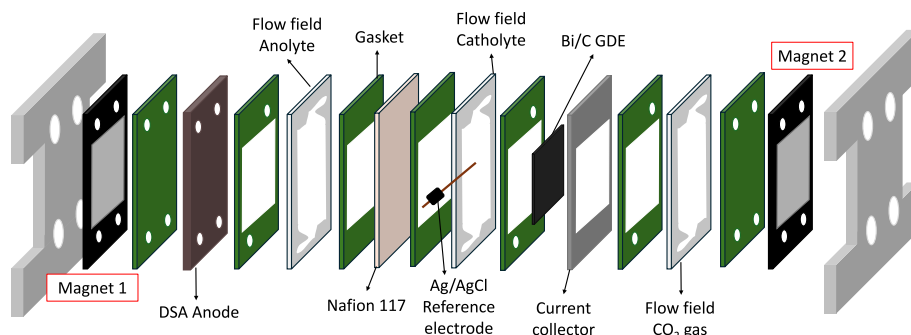


Fig. 3. Schematic of the internal configuration with magnets placed on both the anode and cathode side.

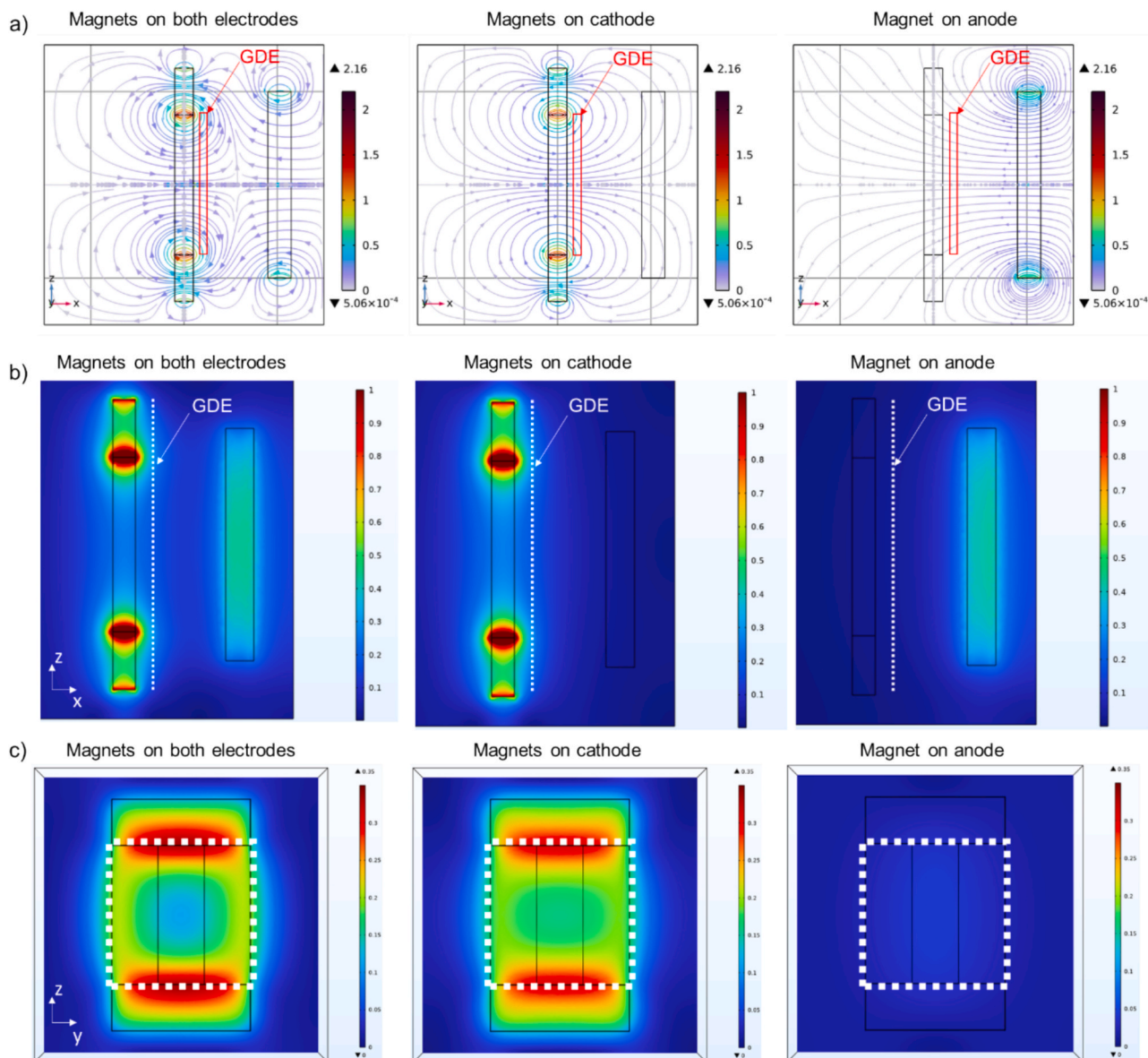


Fig. 4. a) Magnetic field distribution (B vectors) in the x-z plane at the center of the electrolyzer ($y = 0$) showing also B magnitude for all the magnet configurations tested in this study: magnets on both electrodes (left panel), magnet on the cathode side (center panel), and magnet on the anode side (right panel). The red rectangle represents the location of the GDE on the cathode side. b) Magnetic field distribution (B magnitude) in the x-z plane at the center of the electrolyzer for all the magnet configurations. The white dashed line next to the magnet assembly on the left side of the chamber represents the location of the GDE. c) Magnetic field distribution in the y-z plane showing the expected magnetic field on the GDE surface (at a distance of 3.2 mm from the magnets on the cathode). The white dashed rectangle represents the active GDE area (33 mm x 33 mm). Legend represents the B field in Tesla.

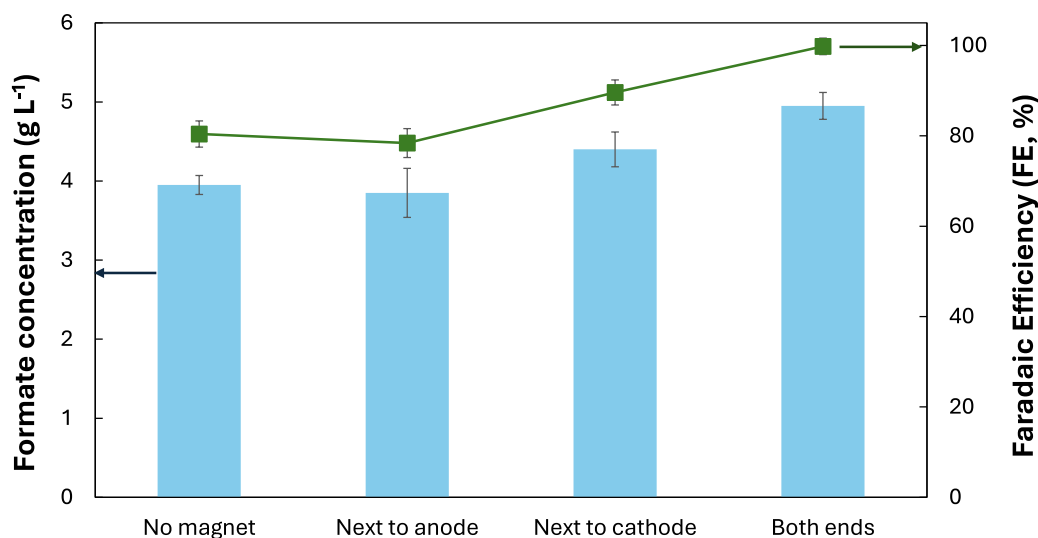


Fig. 5. Formate concentration and FE for different magnet positions in the filter-press reactor.

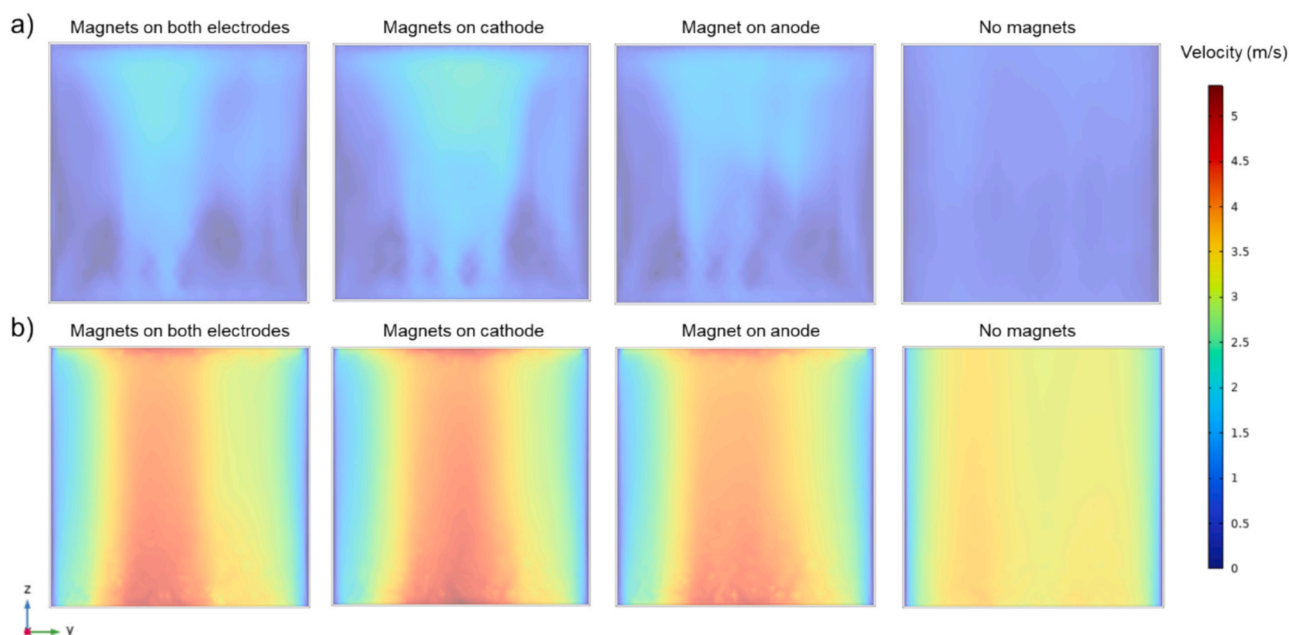


Fig. 6. Electrolyte velocity values at the cathodic compartment for the four magnetic field configurations employed in this work (magnets on both ends, magnet only on the cathode, magnet only on the anode, or no magnet) for a representative catholyte flow rate. a) Velocity values on the GDE surface (at an x distance of 3.2 mm from the magnets on the cathode). b) Velocity values 1 mm away from the GDE surface (at $x = 4.2$ mm from the magnets on the cathode).

the induced magnetic field increases energy consumption, as higher cell voltages are required, thereby raising the total energy required for CO_2 to formate conversion. In the optimal setup, with magnets near both the anode and cathode, energy consumption rises from 277 to 397 kWh kmol^{-1} .

3.2. ERCO_2 for the optimized magnet configuration

As shown in previous results, placing magnets at both ends of the electrochemical cell proves to be the most effective strategy for magnetically enhancing CO_2 electroreduction to formate. This configuration is used to evaluate the impact of the magnetic field on CO_2 conversion performance with varying catholyte flow rates, between 0.57 and 0.07 $\text{mL min}^{-1} \text{cm}^{-2}$.

As observed in Fig. 8, lower flow rates result in higher formate concentrations, consistent with previous works [10]. Regarding the

effect of the magnetic field on CO_2 electroreduction performance, the MHD effect is evident. At lower catholyte flow rates (0.07 $\text{mL min}^{-1} \text{cm}^{-2}$), where natural mixing induced from the catholyte flow is limited, the mass transfer enhancement from the magnets is more pronounced. For example, at a flow rate of 0.57 $\text{mL min}^{-1} \text{cm}^{-2}$, the formate concentration increases by 20 % due to the magnetic field, while at a lower flow rate of 0.07 $\text{mL min}^{-1} \text{cm}^{-2}$, the improvement reaches approximately 50 %, from 18.02 to 27.25 g L^{-1} of formate. These results demonstrate the potential of an external magnetic field to enhance CO_2 electroreduction to formate. In terms of FE, higher values are achieved at larger catholyte flow rates, with an increase of 15–20 % across all cases when the magnetic field is applied.

Moreover, the magnetic field enhances the formate production rate, reaching values of 7.06 and 7.62 $\text{mmol m}^{-2} \text{s}^{-1}$ for 0.07 and 0.15 $\text{mL min}^{-1} \text{cm}^{-2}$, respectively, compared to 4.67 and 6.5 $\text{mmol m}^{-2} \text{s}^{-1}$, without magnets (Fig. 9). On the other hand, as noted previously, the

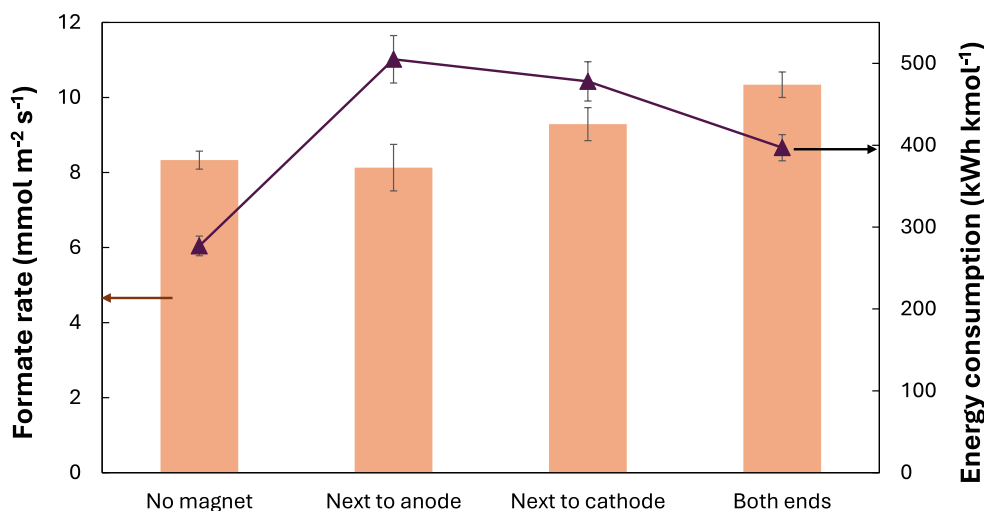


Fig. 7. Formate rate and energy consumption for CO₂ electroreduction to formate with different magnets positions.

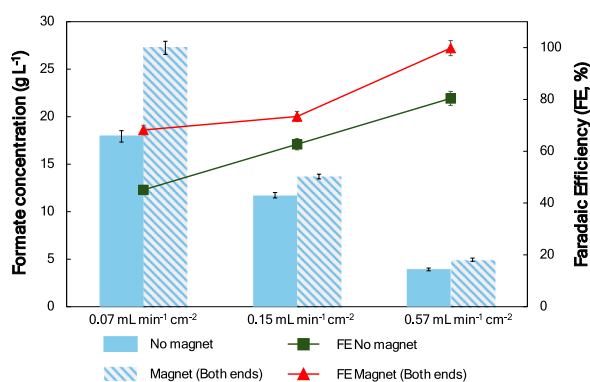


Fig. 8. Formate concentration and FE for varying catholyte flowrates with and without the magnetic field.

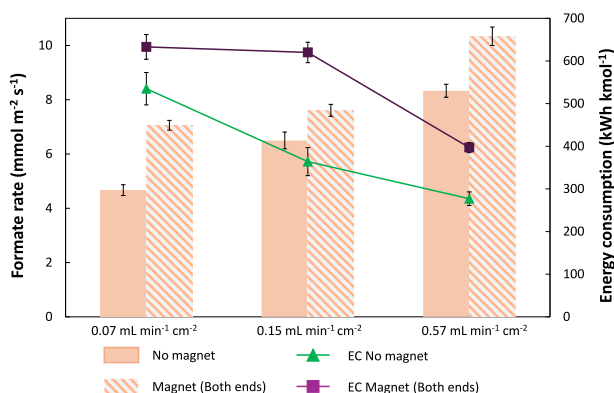


Fig. 9. Formate rate and EC for varying catholyte flow rates with and without the magnetic field.

energy consumption of the system is adversely affected by the magnetic field. For instance, at a flow rate of 0.07 mL min⁻¹ cm⁻², energy consumption increases by approximately 20 %, from 535 to 633 kWh kmol⁻¹, while for the 0.15 mL min⁻¹ cm⁻² scenario, energy consumption rises from 364 to 620 kWh kmol⁻¹, as shown in Fig. 9.

To further investigate the impact of the MHD effect on cathode performance, a modification to the reactor configuration is proposed. Specifically, the Bi-based GDE is placed in close contact with the Nafion

117 membrane to form a Membrane Electrode Assembly (MEA), eliminating the need for a catholyte and feeding a humidified CO₂ stream directly into the cathode compartment. When comparing the formate production results with and without the application of the magnetic field, no significant change is observed. The magnetically influenced operation yields 320 g L⁻¹ of formate, compared to the 312 g L⁻¹ from the non-magnet operation [9], with FEs of 22.8 and 24.8 % respectively. The formate rate decreases from 2.57 to 2.21 mmol m⁻² s⁻¹. Thus, the behavior of this catholyte-less system confirms that the main effect of the applied magnetic field in the electrochemical cell is linked to the MHD effect, which enhances catholyte mixing in the reaction area, thereby reducing mass transfer limitations. This leads to a significant enhancement in CO₂ reduction performance to formate when magnets are applied.

Moreover, in the MEA configuration, the placement of magnets in the electrochemical cell increases energy consumption, rising from 547 to 1100 kWh kmol⁻¹, due to an increase in the overall cell potential. This trend is consistent across all configurations analyzed, where the presence of magnets results in a higher overall cell potential. To better understand the system's behavior, additional electrochemical analyses have been conducted.

Fig. 10.a presents polarization plots for experiments conducted with and without a magnetic field, where different current densities are applied, and both cathode and cell voltages are recorded. As observed, for the same applied current density, the cell potential is higher when magnets are used. Fig. 10.b shows the Tafel plots for the cathode overpotential, highlighting two distinct regions.

To calculate the cathode overpotential, a reference value of -0.35 V (vs. Ag/AgCl) is used, as this is considered the working electrode potential at which the ERCO₂ to formate is thermodynamically feasible using a liquid electrolyte with a pH between 8.5–9 [37,38]. In the low-overpotential region (under 1.5 V vs. Ag/AgCl), the Tafel slopes are steeper for the ERCO₂ operation with the magnetic field. However, in the high-overpotential region (overpotentials over 1.5 V vs. Ag/AgCl), which is more relevant for high current density operations, the Tafel slope for the magnet-assisted setup decreases to 1910 mV/decade, compared to 2011 mV/decade for the conventional configuration. This slight reduction in the Tafel slope suggests improved mass transfer resistance, likely due to the MHD effect, supporting the hypothesis of enhanced ERCO₂ performance resulting from this phenomenon [39]. This hypothesis is supported by the EIS analysis (Fig. S.2). At low potentials (-0.8 V vs. Ag/AgCl), the measurements show that the electrode resistance remains unchanged regardless of whether magnetic fields are applied. However, the system with magnetic fields exhibits a higher resistance from other cell components, which is consistent with the

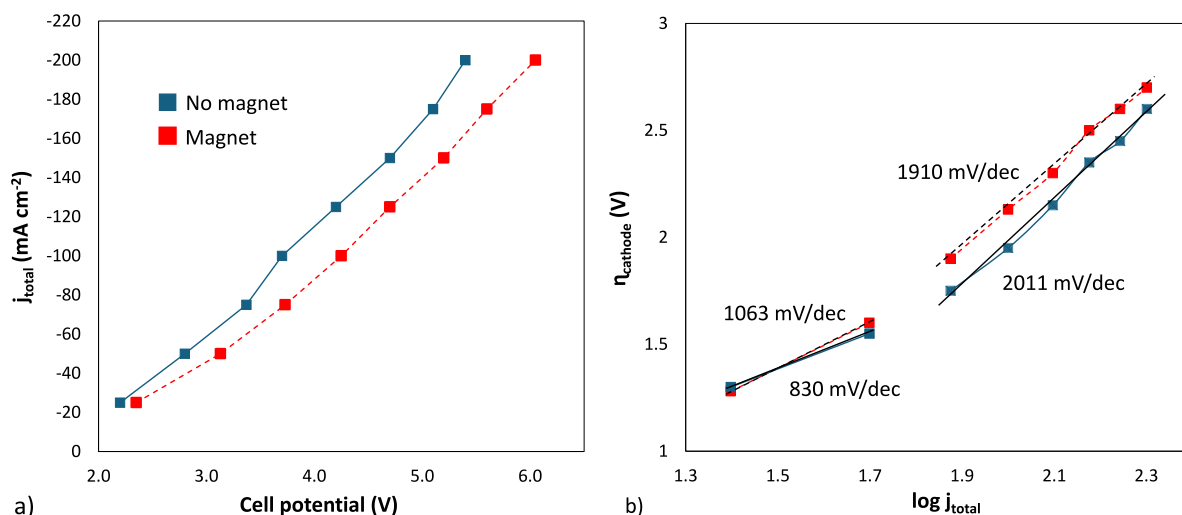


Fig. 10. Polarization plots and Tafel slopes, a) j -V curve with the overall cell potential as a function of the current density with and without the magnetic field, b) Tafel plot with Tafel slopes for both low and high overpotential regions (vs. Ag/AgCl), with and without the magnetic field.

higher cell potentials observed in this case. On the other hand, when the potential is increased to -1.8 V (vs. Ag/AgCl), the Nyquist plots exhibit a characteristic shape of mass transport limitation [40]. Under these conditions, the Nyquist curve for the system with magnetic fields lies below that of the system without magnets, indicating improved mass transport due to the application of the magnetic field.

When considering Fig. 11, it is clear that the increase in cell voltage with the application of a magnetic field is primarily due to changes in the anode overpotential. Despite similar cathode overpotential values in both configurations (with and without magnets), the anode overpotential under the influence of the magnetic field emerges as the main contributor to the overall increase in cell potential. In this case, previous studies have reported that the position of the magnets can significantly influence the cell potential, particularly at the anode. Li et al. [41] showed that when electrodes are oriented vertically and magnets are placed in parallel, the resulting Lorentz force can hinder the detachment of gas bubbles from the electrode surfaces. In the ERCO₂ reactor, the

high rate of O₂ bubble generation at the anode, due to the elevated current density applied, may be similarly affected by the magnetic field. The Lorentz force slows down the detachment of these bubbles, leading to a partial blockage of the electrode surface. This reduces the effective active area in contact with the electrolyte, increases the local electrical resistance, and ultimately raises the anodic overpotential.

Nevertheless, despite the increase in energy consumption, the application of magnetic fields to enhance the ERCO₂ to formate reduction has proven to be a promising approach to maximize the formate production and selectivity, as both concentrations and FE obtained are clearly improved.

4. Conclusions

The coupling of external magnetic fields with electrochemical processes has been proposed to enhance their performance via various effects. However, the application of a magnetic field to the

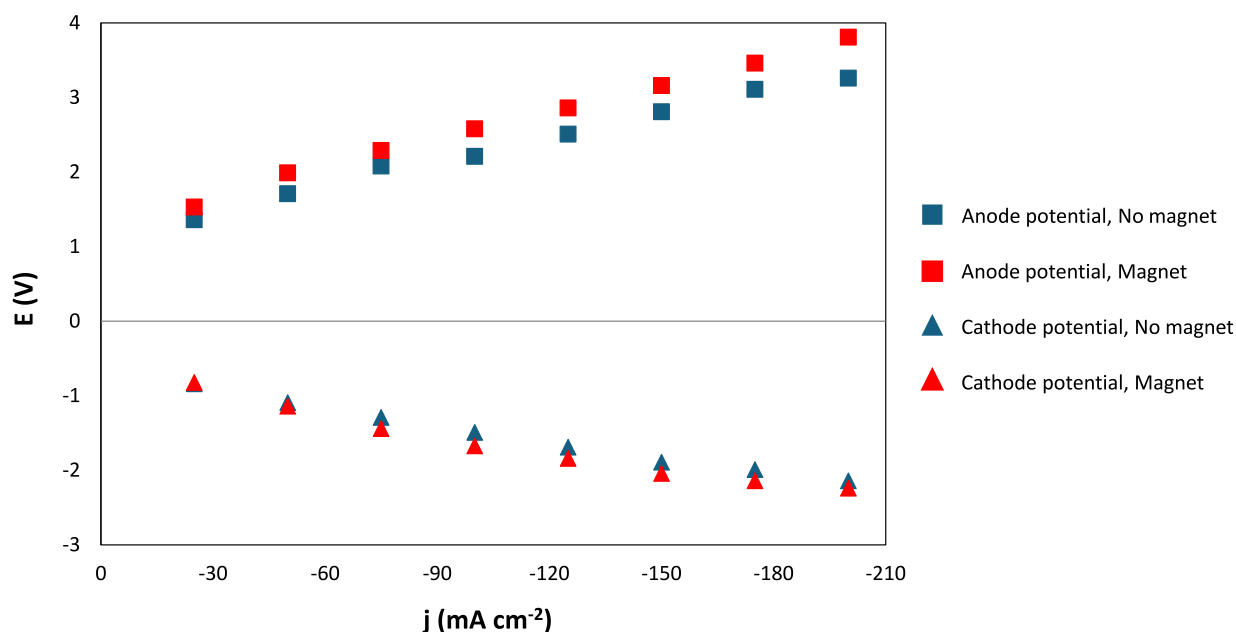


Fig. 11. Anode and cathode potential (vs. Ag/AgCl) evolution for different current densities applied in the system with and without the effect of the external magnetic field.

electroreduction of CO₂ has been scarcely explored in the literature. Specifically, the use of magnetic fields in the conversion of CO₂ to formate has not been previously reported. In this context, this study evaluates the impact of applying a magnetic field to the reduction of CO₂ to formate in a previously characterized filter-press reactor. The aim is to assess performance improvements both experimentally and through magnetic field modeling by strategically positioning magnets outside the electrochemical cell.

Magnetic field modeling reveals that the placement of magnets relative to the working electrode surface significantly influences the magnetic field intensity on this surface. For instance, placing a magnet next to the anode generates a field strength of 20 mT on the GDE. In contrast, the combined action of two magnets paced at opposite ends of the cell results in field values as high as 400 mT. These variations in field strength directly impact the performance of ERCO₂ to formate. Placing a magnet near the anode yields negligible improvements in formate concentration or FE. However, positioning magnets near the cathode or at both ends of the cell increases the formate concentration by over 20 %, reaching 4.4 g L⁻¹ and 4.95 g L⁻¹, respectively, with FE approaching 100 % when magnets are placed at both ends.

These performance improvements can be attributed to the MHD effect, where the magnetic field enhances mass transfer in the cathodic compartment by inducing turbulence in the electrolyte. This effect is particularly pronounced at lower catholyte flow rates, and at the surface of the GDE, as our simulations have reported. Under these conditions, formate concentration increases by up to 50 % at a flow rate of 0.07 mL min⁻¹ cm⁻², rising from 18.02 to 27.25 g L⁻¹ with the magnetic field application. The influence of the MHD effect is further validated using a catholyte-less MEA configuration, where magnet placement does not improve the ERCO₂ to formate process performance.

Despite these improvements in formate production metrics, the application of a magnetic field adversely affects energy consumption. Higher cell voltage values observed in Tafel analysis lead to increased energy consumption in all scenarios involving magnet placement near the electrodes.

Overall, this work represents a promising first step by introducing magnetic fields to enhance the performance of ERCO₂ to formate. It establishes a foundation for future research to further optimize system performance by investigating the effects of magnetic fields on various electrolytes, cell configurations, electrode architectures, and catalytic materials. Indeed, our ongoing work is focused on the detailed explanation of the interplay between the magnetohydrodynamics, mass transfer of chemical species in the cell, and reaction rates, using FEM to describe the phenomena occurring in the entire GDE flow cell. Future studies in the field could be directed towards the optimization of all variables and parameters affected by magnetic fields using validated numerical modeling predictions and machine learning algorithms.

CRediT authorship contribution statement

Jose Antonio Abarca: Writing – original draft, Validation, Methodology, Investigation, Conceptualization. **Xian Wu:** Validation, Investigation, Conceptualization. **Cristina González-Fernández:** Writing – review & editing, Methodology, Formal analysis. **Ioannis H. Karamelas:** Writing – review & editing, Validation, Formal analysis. **Alejandro Gutierrez-Carballo:** Writing – review & editing, Formal analysis. **Joseph A. Gauthier:** Writing – review & editing, Funding acquisition, Formal analysis, Conceptualization. **Gerardine G. Botte:** Writing – review & editing, Supervision, Formal analysis. **Jose Solla-Gullón:** Writing – review & editing, Formal analysis, Data curation. **Angel Irabien:** Writing – review & editing, Resources, Project administration. **Guillermo Díaz-Sainz:** Writing – review & editing, Writing – original draft, Methodology, Investigation, Funding acquisition, Formal analysis, Conceptualization. **Jenifer Gomez-Pastora:** Writing – review & editing, Writing – original draft, Validation, Resources, Methodology, Investigation, Funding acquisition, Formal analysis, Data curation,

Conceptualization.

Declaration of competing interest

The authors declare that they have no known competing financial interests or personal relationships that could have appeared to influence the work reported in this paper.

Acknowledgments

The authors fully acknowledge the financial support received from the Spanish State Research Agency (AEI) through the projects PID2022-138491OB-C31 and PID2022-138491OB-C32 (MICIU/AEI /10.13039/501100011033 and FEDER, UE), TED2021-129810B-C21, and PLEC2022-009398 (MCIN/AEI/10.13039/501100011033 and Union Europea Next Generation EU/PRTR). The present work is related to CAPTUS Project. This project has received funding from the European Union's Horizon Europe research and innovation programme under grant agreement No 101118265. This study was financially supported by Texas Tech University through HEF New Faculty Startup, NRUF Start Up, and Core Research Support Fund. Jose Antonio Abarca gratefully acknowledges the predoctoral research grant (FPI) PRE2021-097200. Cristina González-Fernández thanks the Spanish Ministry of Universities for the Margarita Salas postdoctoral fellowship (grants for the requalification of the Spanish university system for 2021-2023, University of Cantabria), funded by the European Union-NextGenerationEU. Joseph A Gauthier gratefully acknowledges support from The Welch Foundation under Grant Number D-2188-20240404. Jenifer Gomez-Pastora acknowledges support from The Welch Foundation (Grant # D-2236-20250403).

Appendix A. Supplementary data

Supplementary data to this article can be found online at <https://doi.org/10.1016/j.cej.2025.163614>.

Data availability

Data will be made available on request.

References

- [1] I. Masood ul Hasan, L. Peng, J. Mao, R. He, Y. Wang, J. Fu, N. Xu, J. Qiao, Carbon-based metal-free catalysts for electrochemical CO₂ reduction: Activity, selectivity, and stability, *Carbon Energy* 3 (2021) 24–49, <https://doi.org/10.1002/cey2.87>.
- [2] H. Yang, J.J. Kaczur, S.D. Sajjad, R.I. Masel, Performance and long-term stability of CO₂ conversion to formic acid using a three-compartment electrolyzer design, *J. CO₂ Util.* 42 (2020) 101349, <https://doi.org/10.1016/j.jcou.2020.101349>.
- [3] G. Díaz-Sainz, K. Fernández-Caso, T. Lagarteira, S. Delgado, M. Alvarez-Guerra, A. Mendes, A. Irabien, Coupling continuous CO₂ electroreduction to formate with efficient Ni-based anodes, *J. Environ. Chem. Eng.* 11 (2023) 109171, <https://doi.org/10.1016/j.jece.2022.109171>.
- [4] P. Duarah, D. Haldar, V.S.K. Yadav, M.K. Purkait, Progress in the electrochemical reduction of CO₂ to formic acid: A review on current trends and future prospects, *J. Environ. Chem. Eng.* 9 (2021) 106394, <https://doi.org/10.1016/j.jece.2021.106394>.
- [5] K. Fernández-Caso, G. Díaz-Sainz, M. Alvarez-Guerra, A. Irabien, Electroreduction of CO₂: advances in the continuous production of formic acid and formate, *ACS Energy Lett.* 8 (2023) 1992–2024, <https://doi.org/10.1021/acscenergylett.3c00489>.
- [6] D. Wu, F. Jiao, Q. Lu, Progress and understanding of CO₂/CO electroreduction in flow electrolyzers, *ACS Catal.* 12 (2022) 12993–13020, <https://doi.org/10.1021/acscatal.2c03348>.
- [7] F. Proietto, A. Galia, O. Scialdone, Towards the electrochemical conversion of CO₂ to formic acid at an applicative scale: technical and economic analysis of most promising routes, *ChemElectroChem* 8 (2021) 2169–2179, <https://doi.org/10.1002/celec.202100213>.
- [8] H. Pan, X. Jiang, X. Wang, Q. Wang, M. Wang, Y. Shen, Effective magnetic field regulation of the radical pair spin states in electrocatalytic CO₂ reduction, *J. Phys. Chem. Lett.* 11 (2020) 48–53, <https://doi.org/10.1021/acs.jpclett.9b03146>.
- [9] G. Díaz-Sainz, M. Alvarez-Guerra, B. Ávila-Bolívar, J. Solla-Gullón, V. Montiel, A. Irabien, Improving trade-offs in the figures of merit of gas-phase single-pass

- continuous CO₂ electrocatalytic reduction to formate, *Chem. Eng. J.* 405 (2021) 126965, <https://doi.org/10.1016/j.cej.2020.126965>.
- [10] G. Díaz-Sainz, M. Alvarez-Guerra, J. Solla-Gullón, L. García-Cruz, V. Montiel, A. Irabien, CO₂ electroreduction to formate: Continuous single-pass operation in a filter-press reactor at high current densities using Bi gas diffusion electrodes, *J. CO₂ Util.* 34 (2019) 12–19, <https://doi.org/10.1016/j.jcou.2019.05.035>.
- [11] J.A. Abarca, G. Díaz-Sainz, A. Irabien, Inhibiting salt precipitation on the gas diffusion electrode surface in gas-phase CO₂ electroreduction to formate by using an acidic anolyte, *J. CO₂ Util.* 86 (2024), <https://doi.org/10.1016/j.jcou.2024.102897>.
- [12] R.A. Tufa, D. Chanda, M. Ma, D. Aili, T.B. Demissie, J. Vaes, Q. Li, S. Liu, D. Pant, Towards highly efficient electrochemical CO₂ reduction: Cell designs, membranes and electrocatalysts, *Appl. Energy*. 277 (2020) 115557, <https://doi.org/10.1016/j.apenergy.2020.115557>.
- [13] M.S. Sajna, S. Zavahir, A. Popelka, P. Kasak, A. Al-Sharshani, U. Onwusogh, M. Wang, H. Park, D.S. Han, Electrochemical system design for CO₂ conversion: A comprehensive review, *J. Environ. Chem. Eng.* 11 (2023) 110467, <https://doi.org/10.1016/j.jece.2023.110467>.
- [14] S.A. Al-Tamreh, M.H. Ibrahim, M.H. El-Naas, J. Vaes, D. Pant, A. Benamor, A. Amhamed, Electroreduction of carbon dioxide into formate: a comprehensive review, *ChemElectroChem* 8 (2021) 3207–3220, <https://doi.org/10.1002/celec.202100438>.
- [15] S. Lu, F. Lou, Z. Yu, Recent progress in two-dimensional materials for electrocatalytic CO₂ reduction, *Catalysts* 12 (2022) 228, <https://doi.org/10.3390/catal12020228>.
- [16] C. González-Fernández, G. Díaz-Sainz, A. Gutierrez-Carballo, E. Bringas, I. Ortiz, G. G. Botte, J. Gomez-Pastora, Perspectives of magnetically enhanced electroconversion of CO₂ to formic acid and formate, *ACS Sustain. Chem. Eng.* 12 (2024) 3390–3401, <https://doi.org/10.1021/acssuschemeng.3c06654>.
- [17] S. Garg, M. Li, A.Z. Weber, L. Ge, L. Li, V. Rudolph, G. Wang, T.E. Rufford, Advances and challenges in electrochemical CO₂ reduction processes: An engineering and design perspective looking beyond new catalyst materials, *J. Mater. Chem. A Mater.* 8 (2020) 1511–1544, <https://doi.org/10.1039/c9ta13298h>.
- [18] J. Lin, Y. Zhang, P. Xu, L. Chen, CO₂ electrolysis: Advances and challenges in electrocatalyst engineering and reactor design, *Mat. Reports: Energy*. 3 (2023) 100194, <https://doi.org/10.1016/j.matre.2023.100194>.
- [19] Y. Zhang, C. Liang, J. Wu, H. Liu, B. Zhang, Z. Jiang, S. Li, P. Xu, Recent advances in magnetic field-enhanced electrocatalysis, *ACS Appl. Energy Mater.* 3 (2020) 10303–10316, <https://doi.org/10.1021/acsaem.0c02104>.
- [20] S. Luo, K. Elouarzaki, Z.J. Xu, Electrochemistry in Magnetic Fields, *Angew. Chem. Int. Ed.* 61 (2022) e202203564, <https://doi.org/10.1002/anie.202203564>.
- [21] T.C. Player, P.J. Hore, Source of magnetic field effects on the electrocatalytic reduction of CO₂, *J. Chem. Phys.* 153 (2020) 084303, <https://doi.org/10.1063/5.0021643>.
- [22] P. Vensaus, Y. Liang, J.P. Ansermet, G.J.A.A. Soler-Illia, M. Lingenfelder, Enhancement of electrocatalysis through magnetic field effects on mass transport, *Nat. Commun.* 15 (2024) 2867, <https://doi.org/10.1038/s41467-024-46980-8>.
- [23] V. Gatard, J. Deseure, M. Chatenet, Use of magnetic fields in electrochemistry: A selected review, *Curr. Opin. Electrochem.* 23 (2020) 96–105, <https://doi.org/10.1016/j.coelec.2020.04.012>.
- [24] G. Salinas, C. Lozon, A. Kuhn, Unconventional applications of the magnetohydrodynamic effect in electrochemical systems, *Curr. Opin. Electrochem.* 38 (2023) 101220, <https://doi.org/10.1016/j.coelec.2023.101220>.
- [25] K. Roy, P. Devi, P. Kumar, Magnetic-field induced sustainable electrochemical energy harvesting and storage devices: Recent progress, opportunities, and future perspectives, *Nano Energy* 87 (2021) 106119, <https://doi.org/10.1016/j.nanoen.2021.106119>.
- [26] O. Lioubashevski, E. Katz, I. Willner, Magnetic field effects on electrochemical processes: A theoretical hydrodynamic model, *J. Phys. Chem. B* 108 (2004) 5778–5784, <https://doi.org/10.1021/jp037785q>.
- [27] S.S. Bhargava, D. Azmoodeh, X. Chen, E.R. Cofell, A.M. Esposito, S. Verma, A. A. Gewirth, P.J.A. Kenis, Decreasing the energy consumption of the CO₂ electrolysis process using a magnetic field, *ACS Energy Lett.* 6 (2021) 2427–2433, <https://doi.org/10.1021/acsenrgylett.1c01029>.
- [28] M.S. Kodaimati, R. Gao, S.E. Root, G.M. Whitesides, Magnetic fields enhance mass transport during electrocatalytic reduction of CO₂, *Chem Catal.* 2 (2022) 797–815, <https://doi.org/10.1016/j.checat.2022.01.023>.
- [29] N. Karki, I.G. Marquina, J.V. Hemmer, Y. Yu, A.J. Wilson, Suppressing competing solvent reduction in CO₂ electroreduction with a magnetic field, *J. Phys. Chem. Lett.* 15 (2024) 7045–7054, <https://doi.org/10.1021/acs.jpcllett.4c01672>.
- [30] G. Díaz-Sainz, J.A. Abarca, M. Alvarez-Guerra, A. Irabien, Exploring the impact of partial pressure and typical compounds on the continuous electroconversion of CO₂ into formate, *J. CO₂ Util.* 81 (2024), <https://doi.org/10.1016/j.jcou.2024.102735>.
- [31] G. Díaz-Sainz, M. Alvarez-Guerra, A. Irabien, Continuous electrochemical reduction of CO₂ to formate: comparative study of the influence of the electrode configuration with sn and bi-based electrocatalysts, *Molecules* 25 (2020) 4457, <https://doi.org/10.3390/molecules25194457>.
- [32] J.A. Abarca, G. Díaz-Sainz, I. Merino-García, G. Beobide, J. Albo, A. Irabien, Optimized manufacturing of gas diffusion electrodes for CO₂ electroreduction with automatic spray pyrolysis, *J. Environ. Chem. Eng.* 11 (2023) 109724, <https://doi.org/10.1016/j.jece.2023.109724>.
- [33] X. Wu, H. Choe, J. Strayer, J. Gómez-Pastora, M. Zborowski, B. Wyslouzil, J. Chalmers, Numerical modeling and in situ small angle X-ray scattering characterization of ultra-small SPION magnetophoresis in a high field and gradient separator, *Nanoscale* 16 (2024) 7041–7057, <https://doi.org/10.1039/d3nr05589b>.
- [34] J. Strayer, H. Choe, X. Wu, M. Weigand, J. Gómez-Pastora, M. Zborowski, J. Chalmers, Measuring magnetic force field distributions in microfluidic devices: Experimental and numerical approaches, *Electrophoresis* 45 (2024) 743–751, <https://doi.org/10.1002/elps.202300093>.
- [35] J. Antonio Abarca, G. Díaz-Sainz, I. Merino-García, A. Irabien, J. Albo, Photoelectrochemical CO₂ electrolyzers: From photoelectrode fabrication to reactor configuration, *J. Energy Chem.* 85 (2023) 455–480, <https://doi.org/10.1016/j.jechem.2023.06.032>.
- [36] L.M.A. Monzon, J.M.D. Coey, Magnetic fields in electrochemistry: The Lorentz force. A mini-review, *Electrochem. Commun.* 42 (2014) 38–41, <https://doi.org/10.1016/j.elecom.2014.02.006>.
- [37] D. Ewis, M. Arsalan, M. Khaled, D. Pant, M.M. Ba-Abbad, A. Amhamed, M.H. El-Naas, Electrochemical reduction of CO₂ into formate/formic acid: A review of cell design and operation, *Sep. Purif. Technol.* 316 (2023) 123811, <https://doi.org/10.1016/j.seppur.2023.123811>.
- [38] X.V. Medvedeva, J.J. Medvedev, S.W. Tatarchuk, R.M. Choueiri, A. Klinskova, Sustainable at both ends: electrochemical CO₂ utilization paired with electrochemical treatment of nitrogenous waste, *Green Chem.* 22 (2020) 4456–4462, <https://doi.org/10.1039/D0GC01754J>.
- [39] S.S. Bhargava, D. Azmoodeh, X. Chen, E.R. Cofell, A.M. Esposito, S. Verma, A. A. Gewirth, P.J.A. Kenis, Decreasing the energy consumption of the CO₂ electrolysis process using a magnetic field, *ACS Energy Lett.* 6 (2021) 2427–2433, <https://doi.org/10.1021/acsenergylett.1c01029>.
- [40] A. Sacco, Electrochemical impedance spectroscopy as a tool to investigate the electroreduction of carbon dioxide: A short review, *J. CO₂ Util.* 27 (2018) 22–31, <https://doi.org/10.1016/j.jcou.2018.06.020>.
- [41] Y.H. Li, Y.J. Chen, The effect of magnetic field on the dynamics of gas bubbles in water electrolysis, *Sci. Rep.* 11 (2021) 1–12, <https://doi.org/10.1038/s41598-021-87947-9>.